Effect of static scatterers in laser speckle contrast imaging: an experimental study on correlation and contrast

Pedrono Guilherme Vaz, Anne Humeau-Heurtier, Edite Figueiras, Carlos Correia, Joao Cardoso

PAPER • **OPEN ACCESS**

Effect of static scatterers in laser speckle contrast imaging: an experimental study on correlation and contrast

IOP Publishing Phys. Med. Biol. 63 (2018) 015024 (12pp) https://doi.org/10.1088/1361-6560/aa9f3a

Physics in Medicine & Biology

IPEM Institute of Physics and Engineering in Medicine

OPEN ACCESS

PAPER

Effect of static scatterers in laser speckle contrast imaging: an experimental study on correlation and contrast

Pedro G Vaz[1,2], Anne Humeau-Heurtier[2], Edite Figueiras[3], Carlos Correia[1] and João Cardoso[1]

[1] LIBPhys-UC, Department of Physics, University of Coimbra, R. Larga, 3004-516, Coimbra, Portugal
[2] LARIS—Laboratoire Angevin de Recherche en Ingénierie des Systèmes, University of Angers, 62 avenue Notre-Dame du Lac, 49000 Angers, France
[3] International Iberian Nanotechnology Laboratory, Avenida Mestre José Veiga, s/n; 4715-330, Braga, Portugal

E-mail: pvaz@uc.pt

Keywords: laser speckle contrast imaging, speckle correlation, spatial contrast, static scatterers

RECEIVED
7 June 2017

REVISED
20 October 2017

ACCEPTED FOR PUBLICATION
5 December 2017

PUBLISHED
29 December 2017

Abstract

Laser speckle contrast imaging (LSCI) is a non-invasive microvascular blood flow assessment technique with good temporal and spatial resolution. Most LSCI systems, including commercial devices, can perform only qualitative blood flow evaluation, which is a major limitation of this technique. There are several factors that prevent the utilization of LSCI as a quantitative technique. Among these factors, we can highlight the effect of static scatterers. The goal of this work was to study the influence of differences in static and dynamic scatterer concentration on laser speckle correlation and contrast. In order to achieve this, a laser speckle prototype was developed and tested using an optical phantom with various concentrations of static and dynamic scatterers. It was found that the laser speckle correlation could be used to estimate the relative concentration of static/dynamic scatterers within a sample. Moreover, the speckle correlation proved to be independent of the dynamic scatterer velocity, which is a fundamental characteristic to be used in contrast correction.

1. Introduction

Laser speckle contrast imaging (LSCI) is a widely used tool for blood perfusion assessment, with established results in many medical fields (Briers *et al* 2013, Humeau-Heurtier *et al* 2013, Senarathna *et al* 2013). This technique makes it possible to produce two-dimensional perfusion maps of large areas, with good temporal and spatial resolution, at a reasonable cost (Richards *et al* 2013). Along with its non-invasive characteristic, it plays an important role in microcirculation assessment.

LSCI is often used in highly vascularized tissues, like cerebral and retinal tissues, because they contain low concentrations of static scatterers which increases the signal-to-noise ratio (SNR) (Parthasarathy *et al* 2010a, Basak *et al* 2014). However, LSCI is also used in low vascularized tissues, like the forearm (Mahé *et al* 2012), containing high concentrations of static scatterers. Scatterers of this type influence the blood flow evaluation, and should be taken into account when a laser speckle contrast analysis is performed.

In spite of LSCI's large range of applications (Kazmi *et al* 2015b), this technique continues to be a major field of investigation in biomedical imaging (Kazmi *et al* 2015c, Braga and González-Peña 2016, Khaksari and Kirkpatrick 2016a, 2016b, Kirby *et al* 2016, Nadort *et al* 2016) due to its known limitations. The major limitations of LSCI are related to its maximum assessment depth—which is low—along with the lack of quantitative blood perfusion values (Vaz *et al* 2016). Traditional laser speckle imaging is a very superficial assessment technique, in which 95% of the interactions occur up to a tissue depth of 700 μm (Davis *et al* 2014). Diffuse laser speckle contrast (Bi *et al* 2013) and laser speckle tomography techniques have recently been developed (Varma *et al* 2014, Huang *et al* 2015) in order to improve LSCI assessment depth.

The development of a quantitative LSCI method is extremely important for clinical studies (Boas and Dunn 2010). Quantitative results are mandatory for meaningful inter-patient studies, and for the comparison of studies performed under different conditions, or in different institutions. In the quest for quantitative laser speckle imaging, many variations of the original technique have been explored. These methods are mainly based on the use of multi-exposure times (Parthasarathy *et al* 2010b), based on calibration with other devices (Nadort *et al* 2013),

or based on diffuse correlation spectroscopy (Valdes *et al* 2014, Huang *et al* 2015). Despite all these efforts, a fully quantitative laser speckle method, with the ability to correctly determine blood perfusion in units of moving blood volume per volume of tissue per second (e.g. ml/ml/s), is still the main challenge of LSCI research (Kirby *et al* 2016).

LSCI is often performed in a qualitative rather than quantitative way, because speckle signals are influenced by many factors difficult to characterize. Among these factors, we can highlight the scatterers' size, the blood vessel calibre (Kazmi *et al* 2015a), the incident light intensity (Kirby *et al* 2016), the coherence and polarization of the light (Thompson *et al* 2011), the speckle size (Ramirez-San-Juan *et al* 2013), the velocity distribution theoretical models (Duncan *et al* 2008), and the presence of static scatterers (Parthasarathy *et al* 2008). An intensive study of each of these factors is necessary, in order to have a precise knowledge of its influence on the laser speckle contrast signal.

Many works (Parthasarathy *et al* 2008, Mazhar *et al* 2011, Dunn 2012, Ramirez-San-Juan *et al* 2014, Kazmi *et al* 2015b, Khaksari and Kirkpatrick 2016a, 2016b) have discussed and dealt with the effect of static scatterers in LSCI. Almost all of these studies were focused only on the effect of different concentrations of static scatterers in the spatial or temporal contrast values. The present work introduces an in-depth study on the effect of the static and dynamic scatterers, in both laser speckle contrast and correlation signals, with a special focus on the determination of the intensity autocorrelation for a large time delay between laser speckle patterns.

2. Background

In order to explain the influence of differences in static scatterer concentration on LSCI, a short mathematical analysis is required. The autocorrelation function of the laser speckle patterns is often the starting point for the analysis of LSCI, because the dynamic laser speckle information is encoded in time. Hence, the function that relates the field autocorrelation with the intensity autocorrelation (Siegert relation) can be defined as (Vaz *et al* 2016)

$$g_2(\tau) = 1 + \beta|g_1(\tau)|^2, \tag{1}$$

where $g_2(\tau)$ is the intensity autocorrelation function, $g_1(\tau)$ is the field autocorrelation function, and β is a normalization constant that accounts for system imperfections, particularly for the speckles' spatial averaging (Boas and Yodh 1997, Briers *et al* 2013). It should be noted that the Siegert relation is only valid if the light electric field is a random Gaussian variable (Lemieux and Durian 1999). Since this relation has been applied in the past for both ordered flow (Parthasarathy *et al* 2008, Nadort *et al* 2013) and Brownian motion (Briers and Webster 1996, Dunn *et al* 2001), we conclude that it can be applied in our experimental conditions. A good overview of the two statistical models mainly used for ordered flow (Gaussian) and Brownian motion (Lorentzian) can be found in Duncan *et al* (2008).

The original LSCI theory described by Fercher and Briers (1981) has been improved over the years in order to account for many of the factors that affect laser speckle imaging (Vaz *et al* 2016). Among these modifications, the correction factor ρ has been included in the field autocorrelation function as a way to estimate the fraction of static scatterers present in the sample. The ρ value can be defined as (Zakharov *et al* 2009)

$$\rho = \frac{\langle I_s \rangle}{\langle I_s \rangle + \langle I_d \rangle}, \tag{2}$$

where $\langle I_s \rangle$ represents the average light intensity scattered by the static scatterers, and $\langle I_d \rangle$ that scattered by dynamic scatterers.

The inclusion of this new factor results in the separation of the field autocorrelation function into two parts, one for the dynamic scatterers ($g_{1d}(\tau)$) and the other for the static scatterers ($g_{1s}(\tau)$) (Boas and Dunn 2010):

$$g_1(\tau) = (1-\rho)|g_{1d}(\tau)| + \rho|g_{1s}(\tau)|. \tag{3}$$

Static scatterers are expected to produce a constant speckle signal over time, making the static autocorrelation function independent of τ. Moreover, since the static scatterers contribution is always the same within the temporal region of interest, the correlation between consecutive patterns is equal to 1 ($g_{1s}(\tau) = 1$) (Boas and Yodh 1997). Thus, by replacing $g_1(\tau)$ in equation (1) we obtain

$$g_2(\tau) = 1 + \beta\left[(1-\rho)^2|g_{1d}(\tau)|^2 + 2\rho(1-\rho)|g_{1d}(\tau)| + \rho^2\right], \tag{4}$$

$$= 1 + \beta\left[(1-\rho)|g_{1d}(\tau)| + \rho\right]^2. \tag{5}$$

When the time difference (τ) between two speckle patterns is much larger than the scatterers' decorrelation time ($\tau = \Delta t \gg \tau_c$), the dynamic autocorrelation function becomes insignificant ($g_{1d}(\Delta t) \approx 0$). This is equivalent to saying that, in this specific condition, the correlation between two patterns is only dependent on the amount of light scattered by static and dynamic scatterers, yielding Zakharov *et al* (2009)

$$g_2(\Delta t) = 1 + \beta\,\rho^2. \tag{6}$$

Zakharov *et al* (2009) proposed a practical method to estimate ρ using only laser speckle imaging data. Their method starts from the definition of intensity autocorrelation (Fercher and Briers 1981), and substitutes its denominator by the multiplication of the images' spatial average because the they are completely decorrelated:

$$g_2(\Delta t) = \frac{\langle A \circ B\rangle_s}{\langle A\rangle_s \langle B\rangle_s}, \tag{7}$$

where A and B are two consecutive laser speckle images, $\circ$ corresponds to the Hadamard product (element-wise multiplication) and $\langle \ldots \rangle_s$ represents the spatial averaging. This method is only valid when the two speckle images have a temporal gap much greater than the expected decorrelation time. This requirement impedes the use of this method in high speed laser speckle imaging systems like those proposed in Dragojević (2015) and Sun *et al* (2015).

The use of laser speckle correlation as described in equation (7) raises an important theoretical question. This metric is not normalized to the actual image, in contrast to the standard correlation coefficient, which is normalized to the image average. This fact leads to changes in speckle correlation, computed using this method, not only when the image morphology changes but also when the image average changes (for further reference please see the conclusions of Vaz (2016)). This issue turns out to have a strong effect when multiple exposure times are used, if the average light intensity does not remain constant.

The increase of $\langle I_s\rangle$ produces an increase in the decorrelation time (contrast increase) of the speckle pattern (Parthasarathy *et al* 2008, Ramirez-San-Juan *et al* 2014). On the contrary, an increase of the dynamic scattered light leads to a decrease of the decorrelation time, resulting in a lower contrast image. In fact, it is the relation between the light scattered from dynamic and static scatterers that defines the ρ value. This is the basic idea behind the use of correlation to estimate the amount of light reflected by the static/dynamic scatterers. By rearranging the previous equations, we find that ρ can be computed as

$$\rho = \sqrt{\frac{1}{\beta}\left(\frac{\langle A \circ B\rangle_s}{\langle A\rangle_s \langle B\rangle_s} - 1\right)}, \tag{8}$$

and that $g_2(\Delta t)$, expressed in terms of scattered light, is equivalent to

$$g_2(\Delta t) = 1 + \beta\left(\frac{\langle I_s\rangle}{\langle I_s\rangle + \langle I_d\rangle}\right)^2. \tag{9}$$

Figure 1 presents the theoretical relations between the variables involved in this study. The first subfigure, figure 1(a), shows that, at ρ close to 0, the correlation increases slowly with the increase of ρ. On the contrary, for higher ρ values, the correlation changes rapidly for short increases of ρ. This function has been plotted using equation (6) and considering $\beta \approx 0.6$ (see results). Figure 1(b) shows that the evolution of $g_2(\Delta t)$ is approximately linear after an initial low sensitivity zone where the increase of static scattered light does not produce an increase of the correlation. This analysis is only valid when $\langle I_s\rangle$ and $\langle I_d\rangle$ are two independent variables—i.e. when changes in $\langle I_s\rangle$ do not produce any variation in $\langle I_d\rangle$, and vice versa. The x-axis units are expressed in number of times of dynamic scattered light ($\times\langle I_d\rangle$), resulting in $\langle I_s\rangle = 0.5$ for $\langle I_d\rangle = 2\langle I_s\rangle$.

Our study is focused on the determination of the autocorrelation function in very specific conditions. All the experiments have been conducted in order to approximate the computed intensity correlation to equation (6) by using large inter-frame and exposure times. This is equivalent to saying that the $g_2(\Delta t)$ values presented in this work correspond to the autocorrelation function asymptote. This fact contrasts with, for example, quasi-elastic light scattering and diffuse wave spectroscopy (Duncan and Kirkpatrick 2008, Kirkpatrick *et al* 2008), in which the exposure times are very short, and the autocorrelation function profile can be computed with much higher precision.

A laser speckle imaging prototype and an experimental bench test have been developed in order to confirm the relation of equation (9) (figure 1(b)), and to study the effect of $\langle I_s\rangle$ and $\langle I_d\rangle$ on spatial laser speckle contrast.

3. Materials and methods

3.1. Experimental bench

A customized laser speckle device was used to perform this experiment (figure 2). This device uses a coherent light source (BioRay, Coherent Inc.), with an optical power of 40 mW, with a light wavelength of 640 nm, and with an elliptical beam (2.4 × 1.4 mm). The light source was mounted in a cage system and coupled with a vertical polarizer and with a beam expander which was used to control the final beam size. A 45° reflecting mirror was used to direct the laser beam towards the sample.

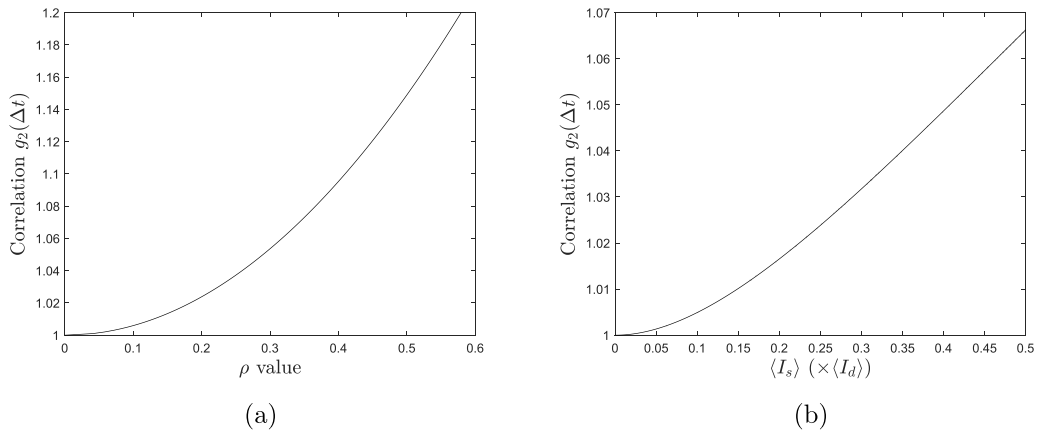

Figure 1. Theoretical relations between: (a) correlation and ρ value (equation (6)) using $\beta \approx 0.6$; (b) light reflected by static scatterers and correlation (equation (9)). The units of (b) x-axes ($\times \langle I_d \rangle$) correspond to the number of times of dynamic scattered light intensity.

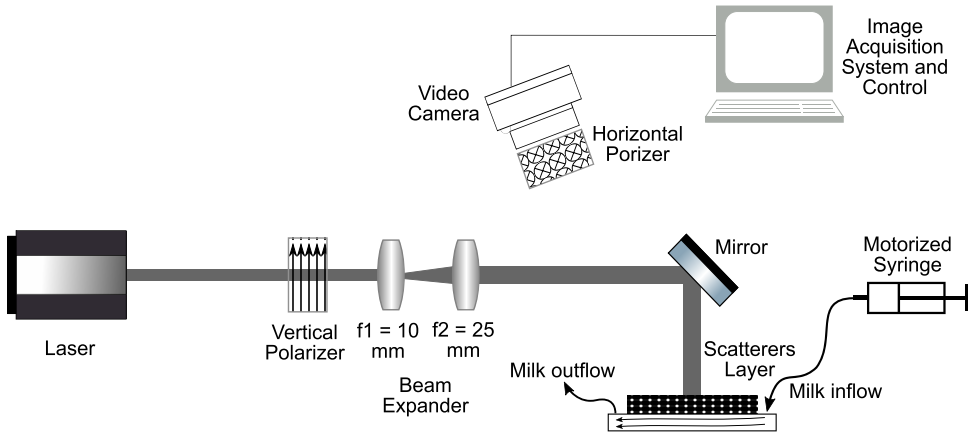

Figure 2. Optical scheme of the laser speckle prototype and bench set-up.

A digital video camera (Pixelink B-741U), connected to a C-mount lens with a fixed focal length of 50 mm (Edmund 67715), was used to record the speckle patterns. An orthogonal polarizer was attached to the camera lens, in order to remove the light directly reflected from the air-sample interface—which contains no valuable information (Basak *et al* 2012).

The camera was programmed with a frame rate of 20 frames per second (fps), a fixed resolution of 320 × 240 pixels and an exposure time of 6 ms. This exposure time was selected because it corresponds to the same as the one used in commercial devices (Perimed PeriCam PSI). The frame rate ensures an inter-frame time of approximately 44 ms. A long inter-frame time is an essential feature of the system since the time difference between two consecutive frames (Δt) must be larger than the scatterers decorrelation time (τ_c), which varies from microseconds to a few milliseconds (Parthasarathy *et al* 2008, Thompson and Andrews 2008).

The optimum system aperture ($f/\#$) was selected so as to match a speckle size (d) of at least two pixels per speckle for each dimension, in order to fulfill the Nyquist theorem (Vaz *et al* 2016). The theoretical equation $d = 1.2(1 + M)\lambda f/\#$ was used to estimate the laser speckle diameter. The system magnification was experimentally computed using an optical resolution target (USAF 1951 1X), and corresponds to $M = 0.2$. Since the camera pixel size is 6.7 × 6.7 μm, the minimum system aperture result is 14.5. An aperture of f/16 was selected because the camera lens only admits discrete values of $f/\#$.

3.2. Phantom

An optical phantom, composed of two distinct parts, has been developed. The bottom part consists of a small longitudinal channel, into which a fluid can be inserted. The top part consists of a doped silicone layer used to simulate various concentrations of static scatterers.

The bottom part has been constructed in acrylic glass, and encloses a channel, with length of 40 mm and a depth of 0.5 mm, with two holes in its ends (inlet and outlet). The channel width is variable, being narrow at

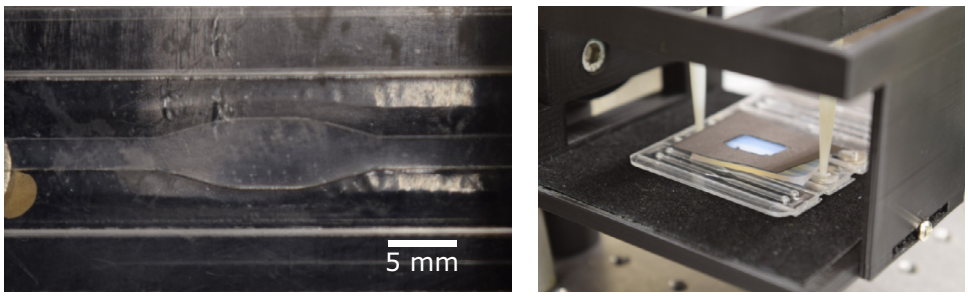

(a) (b)

Figure 3. Photographs of the experimental phantom. (a) Width variation of the channel device, wider in the central part. (b) The channel device below the static scatterers membrane, the micropipette injection system, and the support structure. A black paperboard was used in order to present secondary light reflections.

Table 1. Scatterers concentration of the silicone layers.

Layer	I	II	III	IV	V	VI
Scatterers concentration (mg ml^{-1})	0	0.25	0.5	1	1.5	2

the edges (2 mm) and wider at the central segment (5 mm). Figure 3(a) depicts the phantom acrylic channel, in which the width variations are clearly visible. All the experiments were performed in the central part of the channel, i.e. where its width is 5 mm.

A set of six different silicone layers have been made, with a constant thickness of approximately 1.3 mm and different static scatterer concentrations ($[S_s]$). These layers are composed of a bulk substance (Sylgard® 184 silicone elastomer) doped with particles of TiO_2 (Sigma-Aldrich titanium (IV) oxide, 1% Mn doped, nanopowder, particle size $<$100 nm). The titanium dioxide particles act as static dispersers because they are trapped in the silicone matrix. These materials were chosen because they have been used in other biomedical studies (Bisaillon *et al* 2008, de Bruin *et al* 2010, Tchvialeva *et al* 2011, Nadort *et al* 2016). Table 1 presents the scatterer concentration of each layer, ranging from 0 to 2 mg of TiO_2 per millilitre of elastomer.

Figure 3(b) shows the optical phantom mounted in a 3D printed support. The injection and collection of fluid was performed using two micropipette tips. The injected fluid consists of semi-skimmed milk with a particle concentration (lipids + proteins + carbohydrates) of 99 mg ml^{-1} and particle sizes ranging from 0.1 μm to 2 μm. The use of milk has a number of advantages over the use of blood; specifically, it does not sediment, it is much easier to handle, and presents a behavior similar to intralipid solutions (Waterworth *et al* 1995, Cubeddu *et al* 1997). This fluid has also been used in several optical based studies (Wojtkiewicz *et al* 2009, Figueiras *et al* 2010, Figueiras 2012), and in some LSCI works (Winchester and Chou 2004, Thompson and Andrews 2010). The work from Thompson and Andrews (2010) applied a multi-exposure LSCI to milk, with results similar to those found in red blood cells.

Various concentrations of fluid were used, in order to specify the concentration of dynamic scatterers in the sample ($[S_d]$). The milk was diluted with water in 1:1(50%) and 3:1 (75%) milk:water volume proportions. Additionally, milk was used without dilution (100%) and with the addition of extra static scatterers (200%)—the latter being achieved by adding powdered milk to the semi-skimmed milk (0.1 g ml^{-1}).

The milk was pumped into the phantom using a motorized syringe pump, Razel® scientific instruments model R-99, with several inflows. The applied flows had been previously simulated using multiphysics software, in order to determine the corresponding channel core velocity. The flows used here (table 2) were selected in order to ensure a phantom core speed in the physiological range (Reece *et al* 2013). A detailed description of this simulation can be found in Vaz (2016).

The total light reflected ($\langle I \rangle$) is proportional to the overall concentration of scatterers ($[S]$), meaning that an increase in $[S]$ produces an increase in $\langle I \rangle$. However, variations in $[S_s]$ and $[S_d]$ produce different changes in $\langle I_s \rangle$ and $\langle I_d \rangle$, because the scatterers do not have the same optical properties. The lack of knowledge about the exact relationship between $[S_s]$ versus $\langle I_s \rangle$ and $[S_d]$ versus $\langle I_d \rangle$ prevents the computation of ρ value using this experiment.

3.3. Signal processing details

The β constant had been determined before the use of the phantom, since it is a characteristic value of the developed prototype, and does not depend on the sample. Practically, this constant corresponds to the highest

Table 2. Relationship between the phantom inflow and the fluid velocity in the core of the wider segment.

Case #	Flow ($cm^3\ h^{-1}$)	Core velocity ($mm\ s^{-1}$)
1	0	0
2	1.5	0.26
3	3	0.53
4	7	1.25
5	14	2.50

contrast that the system can achieve. It was computed by using a white paper sheet as sample (Thompson *et al* 2011). The laser speckle contrast was computed in a 5 × 5 pixel region, and β taken as equal to its mean. This process led to a normalization constant of $\beta = 0.596$.

The same sample (white paper sheet) was used to experimentally determine the minimum speckle size. First, the central line of the 2D—power spectral density (PSD) was computed. After that, a Gaussian curve was fitted to this data, and its full width at half maximum (FWHM) taken as the minimum speckle size (Kirkpatrick *et al* 2007). The minimum speckle size determined with the PSD was 2.44 pixels per speckle.

All the combinations of fluid flow, milk concentration and static scatterer layer were analyzed, resulting in 120 video sequences, each of 600 frames (30 s). All the acquisitions were segmented to be limited to the wider channel segment. The speckle correlation has been computed in regions of 5 × 5 pixels, in the same way as laser speckle contrast (see below). For each acquisition, 599 correlation maps (I_{g_2}) have been computed, and the mean ($\bar{I}_{g_2}$) associated with each acquisition.

The modified Tompkins-τ algorithm has been used to exclude the outliers from each data-set, using a two-tailed distribution with a 95% confidence interval. According to this algorithm, the exclusion criterion can be computed as (Dieck *et al* 2005, Anbarasi *et al* 2011)

$$c_{\text{th}} = \frac{1}{\sqrt{n}} \frac{t_{\alpha/2}(n-1)}{\sqrt{n-2+t_{\alpha/2}^2}}, \tag{10}$$

where n is the number of samples, and $t_{\alpha/2}$ is the critical value of a Student's t-distribution of $n-2$ samples, with a degree of confidence α. With the remaining points, the mean ($\overline{g_2}$) and standard deviation (δg_2) of the correlation have been computed for each configuration. An outlier removal algorithm was applied in order to remove possible areas where the phantoms could present imperfections, such as clusters of scatterers or cracks in the channel.

Finally, the speckle contrast has also been computed using the spatial algorithm (s-K) (Vaz *et al* 2016) because it is still the most used in LSCI. The methods used to post-process the contrast maps were the same used for correlation (mean contrast map and outliers removal). The computation element corresponds to 5 × 5 pixels.

4. Results and discussion

4.1. Correlation $g_2(\Delta t)$

For each configuration used in this experiment, the correlation function $g_2(\Delta t)$ has been computed as mean ± standard deviation (discrete points). These data have been plotted as function of static scatterer concentration. In this paper, only a reduced data-set is shown, for concision. The results are presented only for flows #1 ($0\,cm^3\ h^{-1}$), #2 ($1.5\,cm^3\ h^{-1}$), #4 ($7\,cm^3\ h^{-1}$), and #5 ($14\,cm^3\ h^{-1}$). The complete data-set can be found in Vaz (2016).

Figure 4 presents a graphical analysis of the results obtained for the correlation function $g_2(\Delta t)$ where each subfigure represents a different flow and, consequently, a different core velocity. The increase of the static scatterer concentration should produce an increase of the correlation in a range between $1 \leqslant g_2(\Delta t) \leqslant 1+\beta$. However, this full range is only achieved for a variation of ρ from 0 to 1—which, in experimental conditions, is never achieved.

Both theoretical equation and experimental data show different sensitivities to ρ changes (theory) and to $[S_s]$ (experimental data) changes. More specifically, they have low sensitivity for lower ρ and lower $[S_s]$, and high sensitivity for higher ρ and higher $[S_s]$. However, the data shows that our apparatus lacks sufficient sensitivity to detect variations in $[S_s]$ below $1\ mg\ ml^{-1}$. Only for higher concentrations does $g_2(\Delta t)$ start to increase with the increase of static scatterer concentration. Another important remark that can be extracted from these data is that, for exclusively dynamic scatterers ($[S_s] = 0$), the experimental correlation never reaches the unitary value ($g_2(\Delta t) \neq 1$). This is equivalent to saying that even using a transparent silicone membrane ($[S_s] = 0$), there is mutual information between consecutive frames leading to a value of $\langle I_s \rangle > 0$. This evidence supports the fact that theoretical $g_2(\Delta t)$ values are much lower than those computed experimentally, finishing at $g_2(\Delta t) = 1.00$

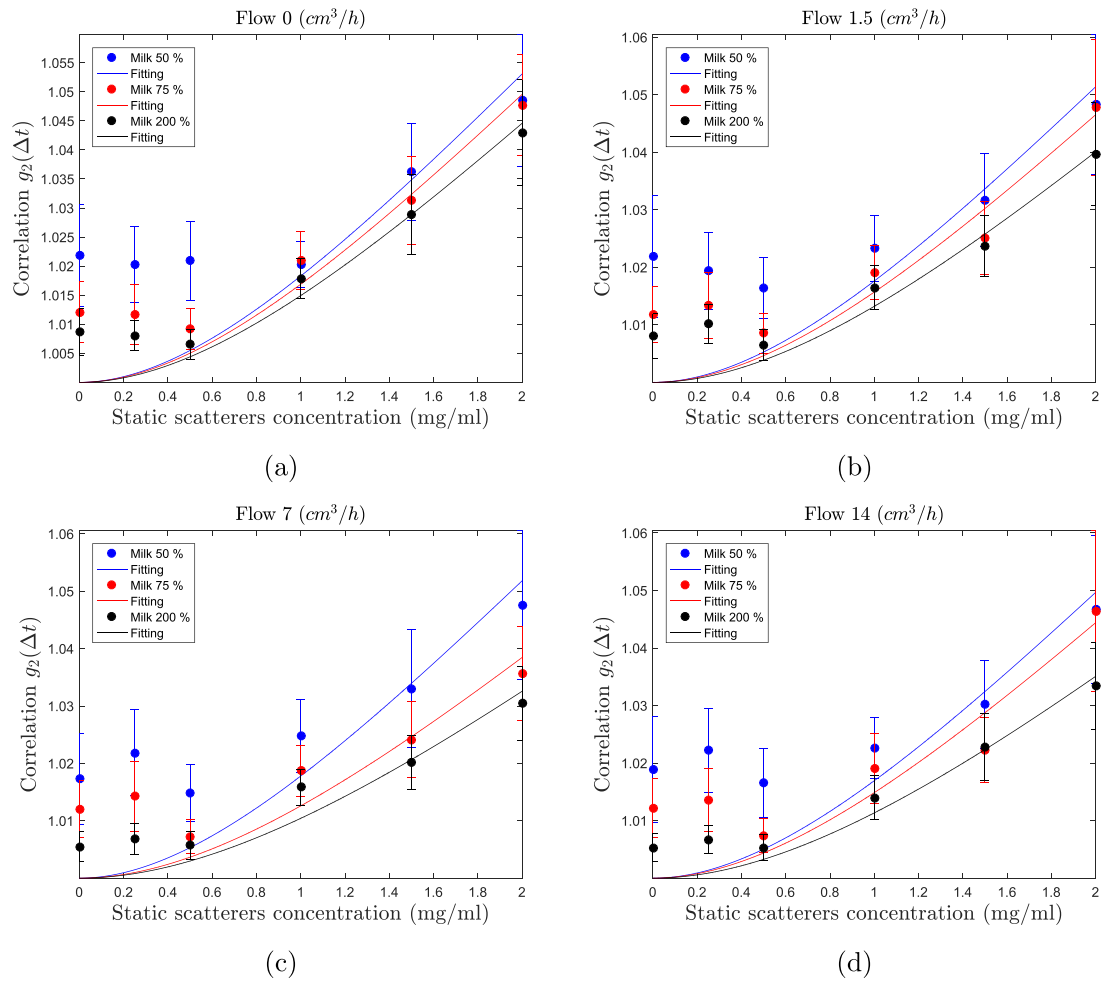

Figure 4. Experimental results obtained for $g_2(\Delta t)$ with the increase of static scatterers concentration. Each sub-figure represents a different fluid flow. The standard deviations have been computed with a minimum of 3165 points. The fitting output has been plotted in solid line.

in the theory, while in the experiment they remain around 1.01. This is due to experimental imperfections like internal reflections of the microchannel. The milk concentration also has an important effect on the minimum detected correlation value, because higher milk concentrations show lower minimum correlation values.

Some conclusions can also be extracted regarding the effect of increasing $[S_d]$. The increase of the milk concentration corresponds to an increase of the dynamic scatterer concentration ($[S_d] \nearrow$)—and, therefore, to an increase of $\langle I_d \rangle$. From figure 4 it can be seen that the correlation for 50% milk is in most cases higher than that for 75% milk, and the correlation for 200% milk is lower than that for the other concentrations. These data show a gradual downward shift, which is a consequence of the theoretically horizontal stretch caused by the increase of $\langle I_d \rangle$. Moreover, this increase has the effect of stretching the x-axis, because the correlation is sensitive to the ratio between static and dynamic scattered light. Graphically, this corresponds to a delay in the correlation function onset or, in other words, the correlation starts to increase at higher values of $[S_s]$.

The error bars correspond to the standard deviation of the correlation for each case. Since an adaptive algorithm has been used to remove the outliers, these standard deviations have been computed with a different number of points. The minimum number of points for each acquisition was 3165, and the maximum 6803. The correlation values computed from samples with higher $[S_d]$ show smaller error bars, which indicates a more precise result. In other words, the presence of a large amount of dynamic scatterers increases the laser speckle signal-to-noise ratio.

Despite the non-equivalence between the scatterer concentration (used in the experiment) and the average reflected light (detailed by the theory), these data have been fitted to the model described by equation (9). The fitting equation was forced to intersect the y-axis at value 1.00 in spite of the experimental issues revealed by our system (the minimum computed correlation being approximately 1.01). The $[S_s]$ was taken as the $\langle I_s \rangle$, and corresponds to the independent variable of the fitting model. The $[S_d]$ was taken as the $\langle I_d \rangle$, and corresponds to the fitting parameter. The fitting output has been plotted as the solid line in figure 4.

Table 3. Fitted values for $[S_d]$.

		Flow ($cm^3\ h^{-1}$)			
		0	1.5	7	14
Milk (%)	50	4.72	4.83	4.80	4.95
	75	4.96	5.18	5.90	5.35
	200	5.34	5.73	6.58	6.27

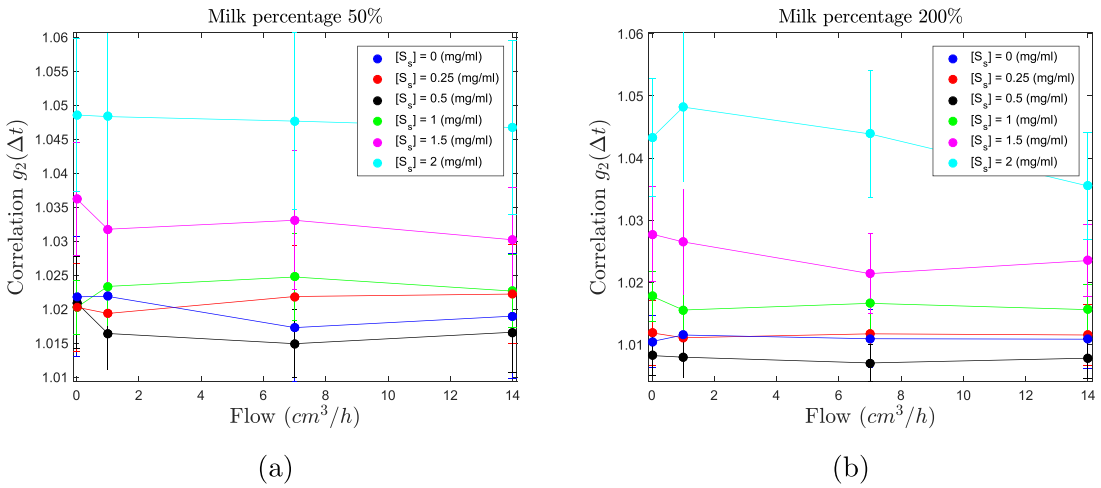

Figure 5. Experimental results obtained for $g_2(\Delta t)$ with the increase of flow. Each sub-figure represents a different milk concentration. The standard deviations have been computed with a minimum of 3165 points. The symbol $[S_s]$ stands for static scatterers concentration.

Table 3 presents the fitting parameter values for each experimental case. The computed dynamic scatterer concentration ($[S_d]$) presents an increase with the increase of milk concentration. The flow changes also produce a variation in the fitted $[S_d]$, but a clear tendency has not been observed.

Regarding the evolution of the correlation as function of the fluid flow (figure 5), an important result can be observed. The increase of the dynamic scatterer velocity results in decorrelation of the image (blurring), which is the same effect caused by a decrease of ρ. This statement could lead us to believe that speckle correlation will be affected by changes in the scatterers' velocity. However, figure 5 shows evidence that changes in the fluid flow do not produce significant variations in $g_2(\Delta t)$.

The same evidence as that we have found in our study has also been concluded in recent works on optical microangiography (Choi *et al* 2016b) and optical coherence tomography (Choi *et al* 2016a). These works also found that, at long time interval measurements, the field autocorrelation between measurements is independent of the particle velocity, but still responds to changes in particle concentration.

In the course of this work, one major issue of the use of $g_2(\Delta t)$ has been identified: the speckle correlation is dependent not only on the image morphology, but also on the image mean intensity. In this experiment, both the exposure time and laser optical power of all the acquisitions were fixed (6 ms and 40 mW). However, the inclusion of different concentrations of scatterers produces slight variations in the image mean intensity. We believe that, in our experiment, this variation does not affect the values of $g_2(\Delta t)$. This should be considered as a study limitation.

4.2. Contrast

The contrast results have been plotted as function of the static scatterers concentration. Figure 6 presents the results of the s-K for the milk concentrations of 50%, 75%, 100% and 200%. By analysing this figure, it can be seen that in most cases, the contrast values for a given concentration of static and dynamic scatterers decrease with the increase of fluid flow, confirming LSCI theory. This situation occurs for almost all the presented cases. The only exceptions are the milk 50% $[S_s] = 2\ mg\ ml^{-1}$, milk 75% $[S_s] = 2\ mg\ ml^{-1}$, milk 100% $[S_s] = 0\ mg\ ml^{-1}$ and milk 200% $[S_s] = 0.25\ mg\ ml^{-1}$.

The contrast value flow dependence is more visible when a milk concentration of 200% is used, due to the reduction of the data error bars. As occurs in the correlation case, this data-set presents higher SNR. It has also been confirmed that the static scatterers concentration has a strong impact in the spatial contrast values. The increment of static scatterers produces an increase of the spatial contrast, which is an effect that can mask fluid

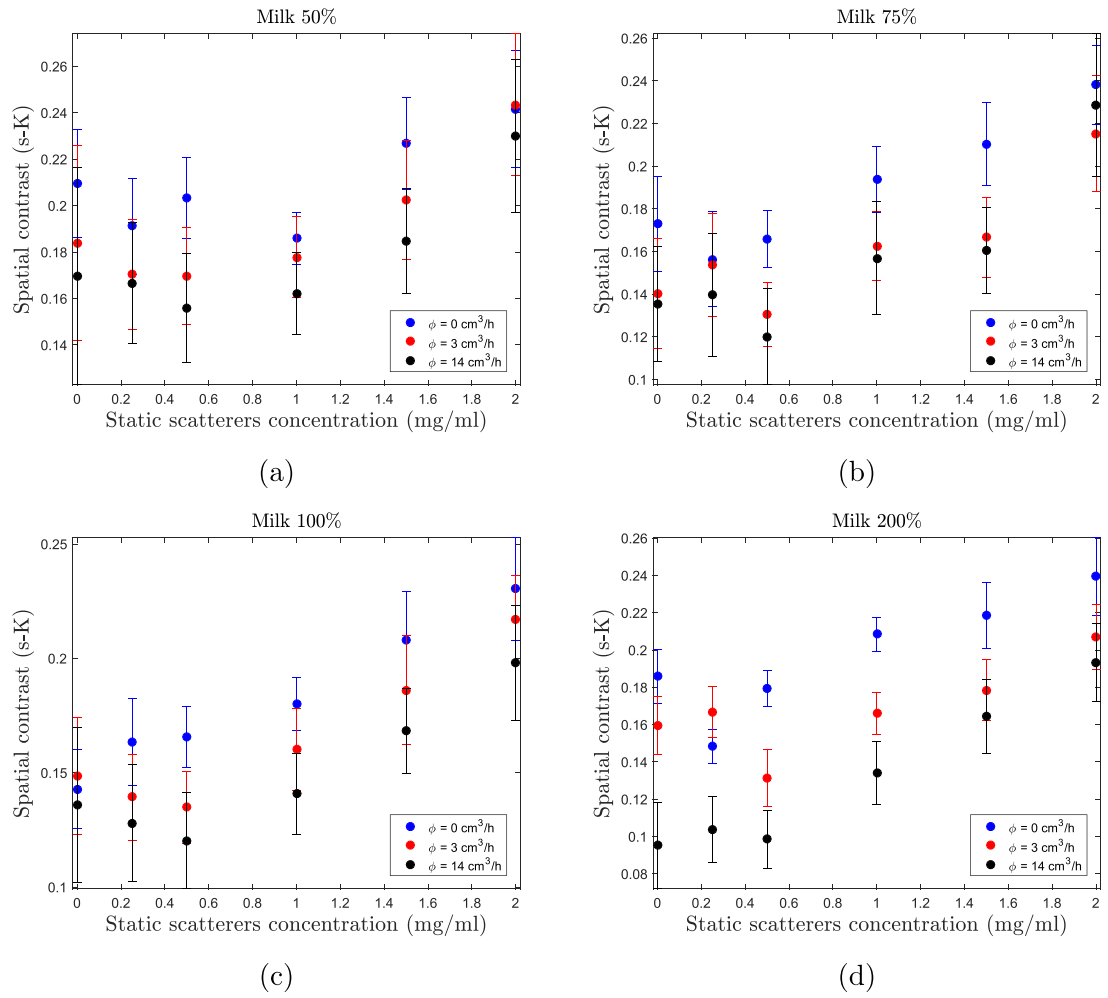

Figure 6. Experimental results obtained for the spatial-contrast (s-K) computation. Each sub-figure represents a different milk concentration. The errorbars have been computed with a minimum of 3602 points. The symbol ϕ stands for flow.

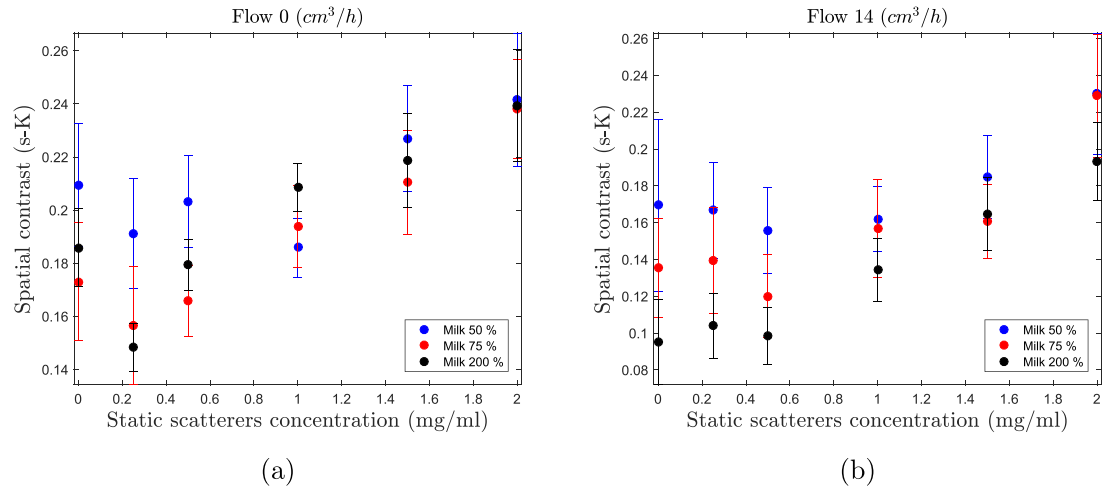

Figure 7. Results obtained for the spatial-contrast (s-K) computation. Each sub-figure corresponds to a different fluid flow. The errorbars have been computed with a minimum of 3602 points.

flow variations. In these data-sets, the influence of $[S_s]$ on contrast values occurs mainly when $[S_s] \geqslant 0.5\,\mathrm{mg\,ml^{-1}}$ are used, making this problem critical when low vascularized tissues are analyzed.

A clear example of $[S_s]$ influence can be extracted from figure 6(c). In this data-set, a contrast value of 0.19 is obtained for a fluid flow of $14\,\mathrm{cm^3\,h^{-1}}$ with $[S_s] = 2\,\mathrm{mg\,ml^{-1}}$, while a contrast value of 0.16 is obtained for a fluid flow of $3\,\mathrm{cm^3\,h^{-1}}$ with $[S_s] = 1.5\,\mathrm{mg\,ml^{-1}}$. According to LSCI, the lower contrast should correspond with

the faster movement; however, this does not occur, due to the $[S_s]$ changes. This example confirms the need to estimate the amount of static scatterers presented in the sample, because the variation of $[S_s]$ leads to erroneous τ_c determination.

Figure 7 presents the s-K results for a specific fluid flow. In this figure, it can be seen that the variation of $[S_d]$ also influences the contrast values. However this effect is visible only for low concentrations of static scatterers ($[S_s] \leqslant 0.5\,\mathrm{mg\,ml^{-1}}$).

5. Conclusion

This study has been conducted in order to analyze the influence of differences in concentration of static and dynamic scatterers on both laser speckle correlation and spatial contrast. Taking advantage of a controlled environment, it has been concluded that both $[S_s]$ and $[S_d]$ influence the speckle correlation and contrast. Moreover, evidence that the laser speckle correlation is independent of the fluid velocity was also identified in these experimental conditions—which is a major requirement for the use of speckle correlation in scatterer estimation.

In future studies, it could be interesting to work on the relation between the scatterer concentration (S) and the mean light intensity that reaches the detector $\langle I \rangle$. An experiment where the dynamic scatterers are removed from the sample and the $[S_s]$ is progressively increased can be used to determine a specific relation between these two variables. The same process could be repeated for $[S_d]$ and $\langle I_d \rangle$, to obtain another independent relation between these two variables. Finally, these two relations should be tested using a variety of scatterer concentrations, in order to determine whether they persist in these conditions.

Moreover, Li and Wang (2017) have studied a different mathematical method of separating the laser speckle signal originating from dynamic and static scatterers. Their method is based on eigen-decomposition filtering, in a technique similar to principal component analysis. The signal components with large eigenvalues are correlated with the signal produced by the static scatterer component. By removing these components, the LSCI signal can be filtered so as to enhance the dynamic scattering signal. Mathematical methods like this should also be considered for future work, in order to improve LSI.

In our study, the analysis of $g_2(\Delta t)$ reveals that the speckle correlation is sensitive to variations in both the dynamic and static scatterer concentrations. However, the $g_2(\Delta t)$ sensitivity to $[S_s]$ and $[S_d]$ is not constant, and depends on their effective concentrations. On one hand, the correlation sensitivity to $[S_d]$ is higher for low concentrations of static scatterers, i.e. for low values of ρ. On the other hand, the correlation sensitivity to $[S_s]$ is higher for high concentrations of static scatterers (high values of ρ).

The effect of fluid flow changes in the speckle correlation is illustrated in figure 5. These data show that the laser speckle correlation is not influenced by variations in the fluid flow. This key conclusion is of extreme importance in the validation of $g_2(\Delta t)$ as a way to estimate the ρ value of the sample. Without this independence, it would be impossible to use the speckle correlation to compute ρ, since $g_2(\Delta t)$ would vary with blood flow variations.

Concluding, this work has demonstrated that the spatial speckle contrast is affected by both the static and dynamic scatterers concentrations apart from the fluid velocity. This fact proves the need to use a correction system in order to make the contrast measurements independent from the static scatterer concentration. The speckle correlation could be an important metric to correct for this effect.

As well as the spatial-contrast algorithm, the temporal and spatio-temporal contrast algorithms have been computed using this data-set. This deserves further work dedicated to comparison between LSCI algorithms.

Acknowledgments

The authors acknowledge the support from Fundação para a Ciência e Tecnologia (FCT—Portugal) for funding a doctoral scholarship (SFRH/BD/89585/2012) and exploratory project IF/01238/2013. The authors acknowledge the Technical University of Tampere (Finland) which kindly provided the microchannel device. Finally, the authors acknowledge the Department of Chemistry of the University of Coimbra (Portugal) and the Center for Neuroscience and Cell Biology (CNC) which provided some of the required lab equipment.

ORCID iDs

Pedro G Vaz https://orcid.org/0000-0003-3490-7789

References

Anbarasi M S, Ghaayathri S, Kamaleswari R and Abirami I 2011 Outlier detection for multidimensional medical data *Int. J. Comput. Sci. Inf. Technol.* **2** 512–6

Basak K, Dey G, Mahadevappa M, Mandal M and Dutta P 2014 *In vivo* laser speckle imaging by adaptive contrast computation for microvasculature assessment *Opt. Lasers Eng.* **62** 87–94
Basak K, Manjunatha M and Dutta P 2012 Review of laser speckle-based analysis in medical imaging *Med. Bol. Eng. Comput.* **50** 547–58
Bi R, Dong J and Lee K 2013 Deep tissue flowmetry based on diffuse speckle contrast analysis *Opt. Lett.* **38** 1401–3
Bisaillon C E, Lamouche G, Maciejko R, Dufour M and Monchalin J P 2008 Deformable and durable phantoms with controlled density of scatterers *Phys. Med. Biol.* **53** N237–47
Boas D and Dunn A 2010 Laser speckle contrast imaging in biomedical optics *J. Biomed. Opt.* **15** 011109
Boas D and Yodh A G 1997 Spatially varying dynamical properties of turbid media probed with diffusing temporal light correlation *J. Opt. Soc. Am.* A **14** 192–215
Braga R A and González-Peña R J 2016 Accuracy in dynamic laser speckle: optimum size of speckles for temporal and frequency analyses *Opt. Eng.* **55** 121702
Briers D, Duncan D, Kirkpatrick S, Larsson M, Stromberg T and Thompson O 2013 Laser speckle contrast imaging: theoretical and practical limitations *J. Bomed. Opt.* **18** 1–9
Briers J and Webster S 1996 Laser speckle contrast analysis (LASCA): a nonscanning, full-field technique for monitoring capillary blood flow *J. Biomed. Opt.* **1** 174–9
Choi W J, Li Y, Qin W and Wang R K 2016a Cerebral capillary velocimetry based on temporal oct speckle contrast *Biomed. Opt. Express* **7** 4859–73
Choi W J, Qin W, Chen C L, Wang J, Zhang Q, Yang X, Gao B Z and Wang R K 2016b Characterizing relationship between optical microangiography signals and capillary flow using microfluidic channels *Biomed. Opt. Express* **7** 2709–28
Cubeddu R, Pifferi A, Taroni P and Torricelli A 1997 A solid tissue phantom for photon migration studies *Phys. Med. Biol.* **42** 1971–9
Davis M, Kazmi S M S and Dunn A K 2014 Imaging depth and multiple scattering in laser speckle contrast imaging *J. Biomed. Opt.* **19** 086001–1
de Bruin D M, Bremmer R H, Kodach V M, de Kinkelder R, van Marle J, van Leeuwen T G and Faber D J 2010 Optical phantoms of varying geometry based on thin building blocks with controlled optical properties *J. Biomed. Opt.* **15** 025001
Dieck R H, Steele W G and Osolsobe G 2005 Test Uncertainty. ASME PTC 19.1-2005 *Technical Report* New York
Dragojević T, Bronzi D, Varma H, Valdes C, Castellvi C, Villa F, Tosi A, Justicia C, Zappa F and Durduran T 2015 High-speed multi-exposure laser speckle contrast imaging with a single-photon counting camera *Biomed. Opt. Express* **6** 2865–76
Duncan D D and Kirkpatrick S J 2008 Can laser speckle flowmetry be made a quantitative tool? *J. Opt. Soc. Am.* A **25** 2088–94
Duncan D D, Kirkpatrick S J and Gladish J C 2008 What is the proper statistical model for laser speckle flowmetry? *Complex Dynamics Fluctuations Biomedical Photonics V* vol 6855 (International Society for Optics and Photonics) (https://doi.org/10.1117/12.760515)
Dunn A K 2012 Laser speckle contrast imaging of cerebral blood flow *Ann. Biomed. Eng.* **40** 367–77
Dunn A K, Bolay H, Moskowitz M A and Boas D A 2001 Dynamic imaging of cerebral blood flow using laser speckle *J. Cerebral Blood Flow Metable* **21** 195–201
Fercher A and Briers J 1981 Flow visualization by means of single-exposure speckle photography *Opt. Commun.* **37** 326–30
Figueiras E 2012 Métodos e instrumentação para fluxometria laser: aplicações à microcirculação sanguínea *PhD Thesis* University of Coimbra
Figueiras E, Ferreira L F R and Humeau A 2010 Phantom validation for depth assessment in laser Doppler flowmetry technique *EOS Topical Meeting Diffractive Optics Koli*
Huang C, Irwin D, Lin Y, Shang Y, He L, Kong W, Luo J and Yu G 2015 Speckle contrast diffuse correlation tomography of complex turbid medium flow *Med. Phys.* **42** 4000–6
Humeau-Heurtier A, Guerreschi E, Abraham P and Mahé G 2013 Relevance of laser Doppler and laser speckle techniques for assessing vascular function: state of the art and future trends *IEEE Trans. Biomed. Eng.* **60** 659–66
Kazmi S, Faraji E, Davis M, Huang Y Y, Zhang X and Dunn A 2015a Flux or speed? Examining speckle contrast imaging of vascular flows *Biomed. Opt. Express* **6** 2588–608
Kazmi S M S, Richards L M, Schrandt C J, Davis M A and Dunn A K 2015b Expanding applications, accuracy, and interpretation of laser speckle contrast imaging of cerebral blood flow *J. Cerebral Blood Flow Metable* **35** 1076–84
Kazmi S M S, Wu R K and Dunn A K 2015c Evaluating multi-exposure speckle imaging estimates of absolute autocorrelation times *Opt. Lett.* **40** 3643–6
Khaksari K and Kirkpatrick S J 2016a Combined effects of scattering and absorption on laser speckle contrast imaging *J. Biomed. Opt.* **21** 76002
Khaksari K and Kirkpatrick S J 2016b Laser speckle contrast imaging is sensitive to advective flux *J. Biomed. Opt.* **21** 076001
Kirby M, Khaksari K and Kirkpatrick S 2016 Assessment of incident intensity on laser speckle contrast imaging using a nematic liquid crystal spatial light modulator *J. Biomed. Opt.* **21** 36001
Kirkpatrick S, Duncan D, Wang R and Hinds M 2007 Quantitative temporal speckle contrast imaging for tissue mechanics *J. Opt. Soc. Am.* A **24** 3728–34
Kirkpatrick S J, Duncan D D and Wells-Gray E M 2008 Detrimental effects of speckle-pixel size matching in laser speckle contrast imaging *Opt. Lett.* **33** 2886–8
Lemieux P A and Durian D J 1999 Investigating non-Gaussian scattering processes by using *n*th-order intensity correlation functions *J. Opt. Soc. Am.* A **16** 1651–64
Li C and Wang R 2017 Dynamic laser speckle angiography achieved by eigen-decomposition filtering *J. Biophotonics* **10** 805–10
Mahé G, Humeau-Heurtier A, Durand S, Leftheriotis G and Abraham P 2012 Assessment of skin microvascular function and dysfunction with laser speckle contrast imaging *Circ. Cardiovasc. Imaging* **5** 155–63
Mazhar A, Cuccia D, Rice T, Carp S, Durkin A J, Boas D, Choi B and Tromberg B J 2011 Laser speckle imaging in the spatial frequency domain *Biomed. Opt. Express* **2** 1553–63
Nadort A, Kalkman K, van Leeuwen T G and Faber D J 2016 Quantitative blood flow velocity imaging using laser speckle flowmetry *Sci. Rep.* **6** 25258
Nadort A, Woolthuis R G, van Leeuwen T G and Faber D J 2013 Quantitative laser speckle flowmetry of the *in vivo* microcirculation using sidestream dark field microscopy *Biomed. Opt. Express* **4** 2347–61
Parthasarathy A B, Tom W J, Gopal A, Zhang X and Dunn A K 2008 Robust flow measurement with multi-exposure speckle imaging *Opt. Express* **16** 1975–89
Parthasarathy A B, Weber E L, Richards L M, Fox D J and Dunn A K 2010a Laser speckle contrast imaging of cerebral blood flow in humans during neurosurgery: a pilot clinical study *J. Biomed. Opt.* **15** 66030–8
Parthasarathy A, Kazmi S and Dunn A 2010b Quantitative imaging of ischemic stroke through thinned skull in mice with multi exposure speckle imaging *Biomed. Opt. Express* **1** 246–59

Ramirez-San-Juan J C, Mendez-Aguilar E, Salazar-Hermenegildo N, Fuentes-Garcia A, Ramos-Garcia R and Choi B 2013 Effects of speckle/pixel size ratio on temporal and spatial speckle-contrast analysis of dynamic scattering systems: implications for measurements of blood-flow dynamics *Biomed. Opt. Express* **4** 1883–9

Ramirez-San-Juan J, Regan C, Coyotl-Ocelotl B and Choi B 2014 Spatial versus temporal laser speckle contrast analyses in the presence of static optical scatterers *J. Biomed. Opt.* **19** 106009

Reece J B, Urry L A, Cain M L, Wasserman S A, Minorsky P V and Jackson R B 2013 Circulation, gas exchange *Campbell Biology* 10th edn (Cambridge: Pearson) ch 42, pp 915–28

Richards L M, Kazmi S M S, Davis J L, Olin K E and Dunn A K 2013 Low-cost laser speckle contrast imaging of blood flow using a webcam *Biomed. Opt. Express* **4** 2269–83

Senarathna J, Member S, Rege A, Li N and Thakor N V 2013 Laser speckle contrast imaging: theory, instrumentation and applications *IEEE Rev. Biomed. Eng.* **6** 99–110

Sun S, Hayes-Gill B R, He D, Zhu Y and Morgan S P 2015 Multi-exposure laser speckle contrast imaging using a high frame rate CMOS sensor with a field programmable gate array *Opt. Lett.* **40** 4587–90

Tchvialeva L, Dhadwal G, Diao D, Lui H, McLean D I and Lee T K 2011 Laser speckle contrast versus depolarization: a solid skin phantom study *Novel Biophotonic Techniques and Applications, Proc. SPIE-OSA Biomedical Optics* ed H Sterenborg and I Vitkin **8090** 809018

Thompson O, Andrews M and Hirst E 2011 Correction for spatial averaging in laser speckle contrast analysis *Biomed. Opt. Express* **2** 1021–9

Thompson O B and Andrews M K 2008 Spectral density and tissue perfusion from speckle contrast measurements *Proc. SPIE* **6847** 68472D

Thompson O B and Andrews M K 2010 Tissue perfusion measurements: multiple-exposure laser speckle analysis generates laser Doppler-like spectra *J. Biomed. Opt.* **15** 027015

Valdes C P, Varma H M, Kristoffersen A K, Dragojevic T, Culver J P and Durduran T 2014 Speckle contrast optical spectroscopy, a non-invasive, diffuse optical method for measuring microvascular blood flow in tissue *Biomed. Opt. Express* **5** 2769–84

Varma H M, Valdes C P, Kristoffersen A K, Culver J P and Durduran T 2014 Speckle contrast optical tomography: a new method for deep tissue three-dimensional tomography of blood flow *Biomed. Opt. Express* **5** 1275–89

Vaz P 2016 Methods for hemodynamic parameters measurement using the laser speckle effect in macro and microcirculation *Phd Thesis* University of Coimbra and University of Angers

Vaz P G, Humeau-Heurtier A, Figueiras E, Correia C and Cardoso J 2016 Laser speckle imaging to monitor microvascular blood flow: a review *IEEE Rev. Biomed. Eng.* **9** 106–20

Waterworth M D, Tarte B J, Joblin A J, Van Doorn T and Niesler H E 1995 Optical transmission properties of homogenised milk used as a phantom material in visible wavelength imaging *Australas. Phys. Eng. Sci. Med.* **18** 39–44

Winchester L and Chou N 2004 Blood velocity measurements using laser speckle imaging *26th Annual Int. Conf. of the IEEE Engineering in Medicine and Biology Society* vol 1 (IEEE)

Wojtkiewicz S, Liebert A, Rix H, Żołek N and Maniewski R 2009 Laser-Doppler spectrum decomposition applied for the estimation of speed distribution of particles moving in a multiple scattering medium *Phys. Med. Biol.* **54** 679

Zakharov P, Völker A C, Wyss M T, Haiss F, Calcinaghi N, Zunzunegui C, Buck A, Scheffold F and Weber B 2009 Dynamic laser speckle imaging of cerebral blood flow *Opt. Express* **17** 13904–17